Fluxes of Heat and Momentum Measured with a Boundary-Layer Wind Profiler Radar–Radio Acoustic Sounding System

WAYNE M. ANGEVINE

Cooperative Institute for Research in Environmental Sciences, University of Colorado/NOAA, Boulder, Colorado

S. K. AVERY

University of Colorado, Boulder, Colorado

W. L. ECKLUND AND D. A. CARTER

NOAA Aeronomy Laboratory, Boulder, Colorado

(Manuscript received 22 January 1992, in final form 10 July 1992)

ABSTRACT

A 915-MHz boundary-layer wind profiler radar with radio acoustic sounding system (RASS) capability has been used to measure the turbulent fluxes of heat and momentum in the convective boundary layer by eddy correlation. The diurnal variation of the heat flux at several heights between 160 and 500 m above ground level and values of the momentum flux for 2-h periods in midday from 160 to 1000 m are presented, as well as wind and temperature data. The momentum flux is calculated both from the clear-air velocities and from the RASS velocities, and the two results are compared.

1. Introduction

a. Instrument and setup

During the summer and fall of 1991 the National Oceanic and Atmospheric Administration (NOAA) Aeronomy Laboratory operated a boundary-layer wind profiler–radio acoustic sounding system (RASS) at Platteville, Colorado. The purpose of the experiment was to determine whether this instrument could be used to measure profiles of heat and momentum fluxes as well as the more usual wind and temperature profiles. We present here the results of that experiment.

The boundary-layer wind profiler was developed by the NOAA Aeronomy Laboratory and is described in Ecklund et al. (1988). It is a relatively compact and portable system operating at a frequency of 915 MHz. The radar uses scattering from refractive-index fluctuations in the clear air to measure the winds. Basic parameters are shown in Table 1. For this experiment, the microstrip antenna was mounted on a mechanically steered platform built by the National Center for Atmospheric Research.

A RASS measures temperature with a Doppler radar and one or more acoustic sources (Matuura et al. 1986; Currier et al. 1988; May et al. 1988; May et al. 1990). The acoustic sources are located near the radar antenna, and the radar measures the speed at which the acoustic disturbance propagates. Recently, the Aeronomy Laboratory has devised several enhancements to RASS (Angevine et al. 1993). The most important of these is the ability to measure the acoustic velocity and the wind velocity simultaneously. This is key to the heat flux measurement.

The radar is set to cycle through four or five different beam directions in sequence. Four of the beam positions are separated by 90° in azimuth (in this case the four cardinal directions are used) at equal zenith angles (10° here). The fifth, optional position points vertically. Generally, RASS measurements have been made with vertically pointing beams. In this experiment, we measured the acoustic velocity as well as the wind velocity on all four or five beams in order to sample the temperature as often as possible.

The radar was operated at 60-m vertical resolution, and the height range covered was from 160 to 914 m. The sampling time for each measurement was about 30 s, and the total time for each measurement was about 40 s, including time for calculations and for the antenna to move and stabilize.

The RASS technique relies on a Bragg match between the acoustic waves and the radar waves. The requirement is that the acoustic wavelength must be one-half the radar wavelength. Since the temperature

Corresponding author address: Wayne M. Angevine, NOAA Aeronomy Laboratory, R/E/AL3, 325 Broadway, Boulder, CO 80303.

TABLE 1. Boundary-layer profiler–RASS parameters.

Frequency	915 MHz
Peak power	500 W
Antenna	Microstrip array
Beamwidth	9°
Acoustic frequency	2000 Hz (nominal)
Acoustic power	30 W

and wind vary with height, the acoustic wavelength also varies. The acoustic source must therefore emit a band of frequencies to cover the Bragg matching condition over the entire height range. Several types of acoustic excitation have been used with RASS, including short acoustic pulses and linear frequency modulation. In this experiment, we used a method that we call "random hop." The acoustic frequency is chosen randomly from within a selected window. A new frequency is selected every 25 ms. The frequency window was 2020–2180 Hz, corresponding to a temperature range of 0°–45°C.

The Platteville site is located atop a shallow ridge at 1523 m above sea level. Vegetation is limited to low grasses with widely spaced stands of trees.

We note that the operating mode used in this experiment is not optimal for any individual measurement with this system. For example, the average height coverage of the RASS could be increased by 300–400 m by using only the vertical radar-beam direction, since the acoustic sources were directed vertically and their half-power beamwidth is only about 10°. On the other hand, the wind measurements could be made to much higher heights if the system was not also running as a RASS, since computer memory limitations restrict the number of range gates that can be used in the RASS mode. The operating mode was chosen to explore the use of the system for a large set of measurements.

b. *Previous results*

A number of experiments have been done previously with other remote and in situ sensors in conditions comparable to those of this experiment. A brief summary of those results follows.

Rabin et al. (1982) reported measurements with dual Doppler radars in a cloudless convective boundary layer in Oklahoma. They found mean momentum fluxes of about 0.2 $m^2 s^{-2}$ in winds of about 15 $m s^{-1}$. Kropfli (1986) made measurements of the momentum flux in the convective boundary layer in Colorado with single X- and K-band Doppler radars. Average values of the flux over 70 min were reported as 0.5–1 $m^2 s^{-2}$ in mean winds of around 5 $m s^{-1}$. The Minnesota experiment (Kaimal et al. 1976) also reported values of the mean momentum flux over 75-min periods as 0.5–1 $m^2 s^{-2}$ in mean winds of about 10 $m s^{-1}$. Heat fluxes in midday were 100–200 $W m^{-2}$ near the surface and decreased with height, dropping to zero near the middle of the boundary layer. These measurements were taken with a 32-m tower and tethered balloons. Doppler lidar measurements (Gal-Chen et al. 1991) in Kansas in July 1987 showed momentum fluxes in the mixed layer of around 0.5 $m^2 s^{-2}$ in mean winds of around 15 $m s^{-1}$.

2. Results

The profiler–RASS combination measures winds and temperature, and from these the heat and momentum fluxes can be derived. We present here the results of these measurements and the techniques used to calculate them. The quantities were calculated over 2-h bins, producing 2-h average winds, temperatures, and fluxes for each day, and then composites were formed of these bins over 2-week periods. These results are from days 164–177 (13–26 June), a period that includes the summer solstice. The weather was similar for all 14 days. The only major difference between the days was in the strength and timing of the afternoon rain showers that occurred on some days.

The radar measures the fall speed of hydrometeors if they are present. In Colorado in the summer, there are often thundershowers in the afternoon. The data processing used for this experiment makes no specific effort to remove data points contaminated by rain, so measurements during the afternoon hours of approximately 1500–1700 MST in this dataset are affected by rain.

In all figures, each time point represents a 2-h average over the 14 days. The 2-h average period is centered about the indicated local standard time.

a. *Winds*

The horizontal winds were computed by subtracting the radial velocities from adjacent measurements of the coplanar beam pairs (east–west or north–south) and dividing by twice the sine of the zenith angle; for example,

$$u = \frac{u_{r1} - u_{r2}}{2 \sin\theta}, \tag{1}$$

where u is a representative horizontal velocity, u_r are the radial velocities in the two directions, and θ is the zenith angle. Similarly, the vertical winds were computed by adding the radial velocities from the coplanar pairs and dividing by twice the cosine of the zenith angle; for example,

$$w = \frac{u_{r1} + u_{r2}}{2 \cos\theta}, \tag{2}$$

where w is the vertical velocity. Outliers more than three standard deviations from the median over each 2-h bin were removed from both the horizontal and vertical wind time series.

Figure 1 shows the average horizontal wind speed and direction profiles. In this period, the average winds

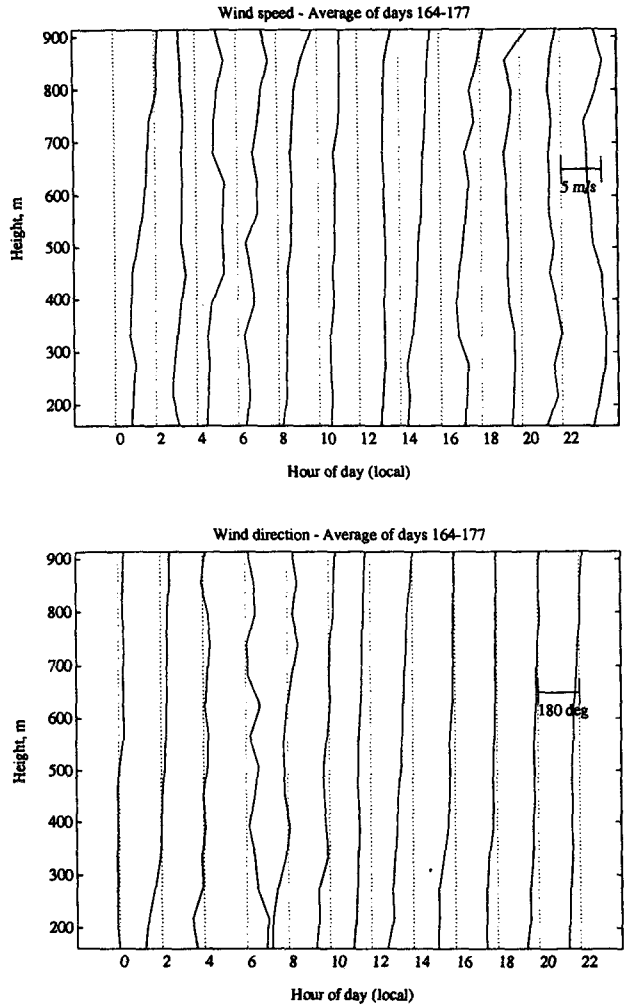

FIG. 1. Average horizontal wind speed and direction profiles for 2-h time bins averaged over 14 days (13–26 June 1991). In the speed plot, the dotted line denotes zero for each time, and the spacing between dotted lines is 5 m s^{-1}. In the direction plot, the dotted line denotes 0° (northward) and the spacing between dotted lines is 180°. A reading to the left of the dotted line for that time is a negative angle.

are fairly light and steady, and primarily toward the north. There are no strong shears in the wind speed. The direction, however, veers with height during most times, as would be expected in the boundary layer.

Figure 2 shows the vertical wind velocity and standard deviation time series. The vertical velocity is generally slightly downward. Downward velocities are often measured with these radars, and the cause is still under discussion. As expected, the standard deviation is larger during midday than in other periods. The velocity is more strongly downward from 1500 to 1700, due to rain showers on some of the days of the period. In precipitation, the radar measures the fall speed of the hydrometeors rather than the wind velocity. The large deviations measured during the hours around sunrise (0400–0800) in the upper heights are an anomaly due to poor radar reflectivity at those times, when the atmosphere is very quiet.

b. Temperature

The virtual temperature T_v can be determined (to a good approximation) in each profiler range gate from the measured speed of sound C_a and the measured vertical wind speed w (see, for example, North and Peterson 1973):

$$T_v(°\mathrm{C}) = \frac{(C_a - w)^2}{401.92} - 273.16. \qquad (3)$$

The temperature was computed according to (3) using simultaneously measured vertical velocities. Velocity measurements from coplanar beam pairs were combined to produce a vertical acoustic velocity and a vertical wind velocity (2). This results in an equivalent sample spacing of 60 s in the five-beam mode. Outliers more than three standard deviations from the median over each 2-h time bin were removed from the temperature time series.

Figure 3 shows the virtual temperature as measured by the RASS in diurnal time series. The temperature shows a diurnal variation, which decreases with height.

In Fig. 4, the virtual potential temperature as calculated using the pressure versus height relationship from the standard atmosphere (NOAA 1976) and referenced to the ground (rather than to sea level) is shown. The lapse rate at the observed heights is subadiabatic until 0900–1100, at which time it is mildly superadiabatic up to 700 m. It becomes subadiabatic again during the 1500–1700 time bin. Since the lapse

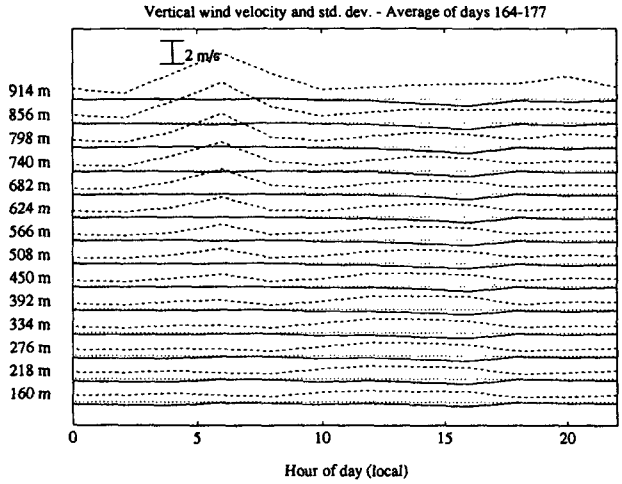

FIG. 2. Vertical wind velocity and standard deviation averaged as in Fig. 1. Height interval is 60 m. The solid line is the mean velocity; the dashed line is the standard deviation; and the dotted line is the zero reference at each height. The spacing between each zero reference line is 2 m s^{-1}. Note the downward velocity in late afternoon due to the sensitivity of the radar to rain showers.

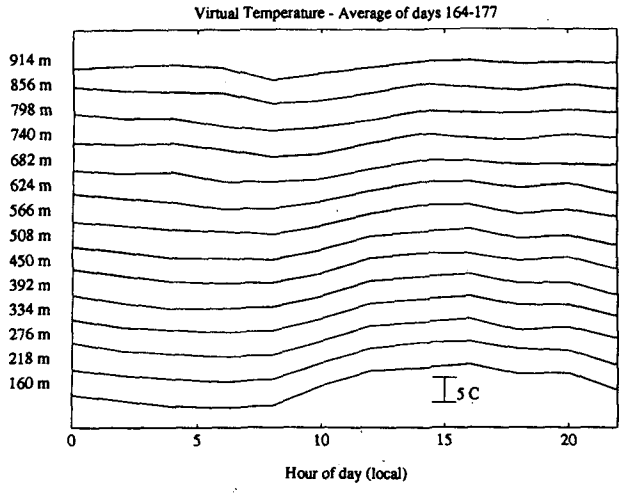

FIG. 3. Virtual-temperature time series averaged as in Fig. 1. Each height is offset by 5°C. The horizontal axis represents 15°C at the lowest height.

rate is not measured all the way to the ground, it is not possible to determine the stability of the measured layer (Stull 1991), and in fact, it is quite likely that convective turbulence is present earlier than 0900 at some levels.

c. *Heat flux*

The heat flux is computed by the technique of Peters et al. (1985):

$$Q = \rho \frac{c_p}{2} [\mathrm{cov}(T'_v, w')(-1) + \mathrm{cov}(T'_v, w')(1)]. \quad (4)$$

Here ρ is the air density; c_p is the heat capacity of air at constant pressure; and the argument of the covariance is the lag between the temperature and the vertical velocity. The covariance of the virtual temperature and the radial wind velocity were calculated over each 2-h time bin. The covariance at zero lag is contaminated by errors in the radial wind measurement, which enters into the temperature measurement as well by way of the vertical wind correction (3). To correct for this, the heat flux is computed by interpolating between the covariances at plus and minus one lag (one measurement time, in this case 60 s). This probably results in an underestimate of the actual flux, since the sample time is comparable to the expected residence time of the major eddies. This technique has the advantage of rendering the final result less sensitive to measurement errors, since errors in the wind measurement that persist for one sample period or less will be removed. As was done for the preceding temperature calculations, the virtual temperature T'_v and the vertical velocity w' used in this calculation were calculated from vertical beams and from coplanar pairs, rather than from individual oblique beams.

This measurement represents the heat flux on time scales longer than the radar sample time (60 s per equivalent vertical measurement) and shorter than the 2-h time bin. The total heat flux is larger than that measured because of contributions on smaller time scales.

Since the virtual temperature rather than the kinetic temperature is used, the heat flux produced by this calculation differs from the sensible heat flux by approximately

$$0.608 - C_p(\overline{Tq'w'} + \overline{qT'w'}), \quad (5)$$

where q is the specific humidity and q' is its fluctuation. In the conditions of this experiment, q is quite small, never more than 0.02. If w' and q' were very well correlated, the first term above could be significant. We cannot draw a firm conclusion about the size of the correction in this experiment, since we lack humidity measurements.

Figure 5 shows the heat flux as computed from the radar–RASS measurements. The time series shows a clear diurnal variation of turbulent heat flux with a reasonable magnitude. The peak heat flux at the lowest height is about 120 W m^{-2}. This represents the average flux over 2-h periods at midday, averaged over 14 days. When the 14-day composite average is formed, values of the heat flux exceeding 400 W m^{-2} in magnitude are excluded. Therefore, the composite at any given height and time may include values for fewer than 14 days. Measurements between 0400 and 0800 h are probably not reliable because of the aforementioned poor radar reflectivity.

The heat flux is shown for fewer heights than the wind and temperature profiles because second-order

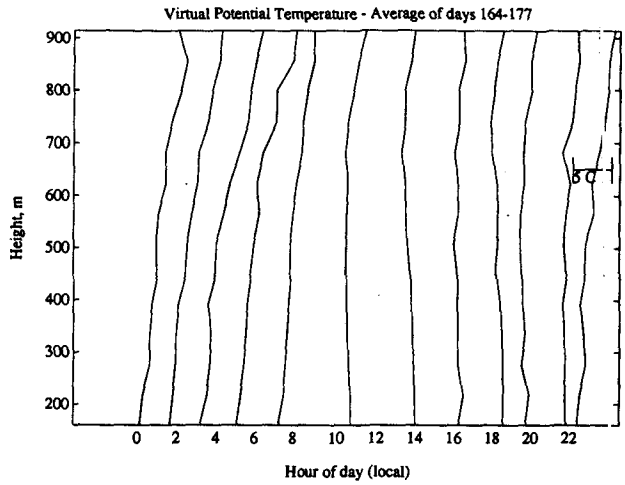

FIG. 4. Virtual potential temperature as calculated using the standard atmosphere and referenced to the ground, averaged as in Fig. 1. Each 2-h time bin is offset 5°C.

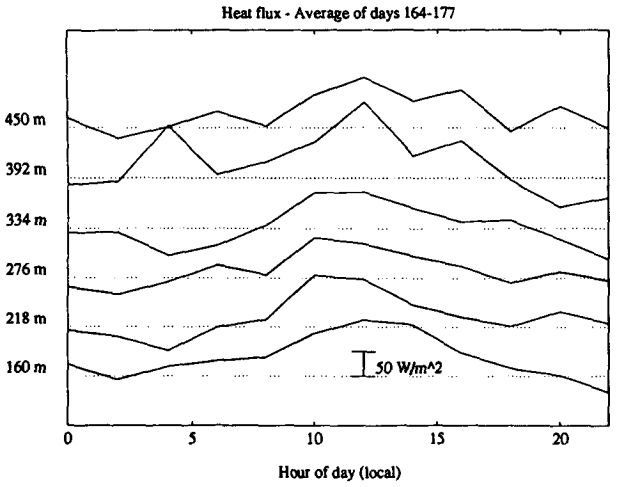

FIG. 5. Heat flux for the lowest six heights. The dotted line is the zero reference for each height. Each height is offset by 100 W m^{-2}. The top two heights show increasing uncertainty due to poor RASS height coverage.

quantities such as fluxes are much more sensitive to data quality and availability. As we mentioned earlier, the height coverage of the RASS in this experiment was degraded by using the oblique radar beams with a narrow-beam acoustic source. This height coverage should not be taken as representative of the capability of the instrument.

d. Momentum flux

The turbulent vertical flux of horizontal momentum on scales larger than the radar resolution volume is computed by the method of Vincent and Reid (1983):

$$\overline{u'w'} = \frac{\overline{u_{r1}'^2} - \overline{u_{r2}'^2}}{2\sin 2\theta}, \tag{6}$$

where u_r' are the radial-velocity fluctuations in two coplanar beam directions and θ is the zenith angle of the beams. This method uses the difference of the velocity variance measured by two beams aimed at the same zenith angle and opposite azimuth angles. The velocity variance is governed by the mean motion of all the scatterers (in this case, refractive-index fluctuations) in the volume illuminated by the radar. A similar technique (Reid 1987) is used to compute the subresolution momentum flux by subtracting the mean spectral widths of the two coplanar beams:

$$\overline{u'w'} = \frac{\sigma_1^2 - \sigma_2^2}{2\sin 2\theta}, \tag{7}$$

where $\sigma_{1,2}$ are the Doppler spectral widths measured by beams in two coplanar directions. The spectral widths measure the relative motions of the scatterers within the illuminated volume. Both methods require the assumption that the statistics of the wind in the volumes illuminated by the two beams are the same.

Figure 6 shows the momentum flux. The plots are for the component aligned with the wind and the component across the wind (+90° from the wind direction). The wind direction used is the average over the three lowest radar range heights for each 2-h period. The flux is calculated for time scales longer and shorter than the radar sampling time (and therefore also for length scales larger and smaller than the radar resolution volume). The longest scale represented is limited by the 2-h time window. Figure 6a shows the fluxes for scales larger than the radar resolution; Fig. 6b is for smaller scales; and Fig. 6c is the total flux on all scales less than 2 h. The total flux is the vector sum of the large- and small-scale fluxes. The solid lines are computed from the clear-air wind velocities, and the dashed lines are computed from the acoustic velocities measured by the RASS. Six heights are plotted for the acoustic-derived fluxes, although the higher heights are less reliable. The fluxes are plotted only for the middle of the day. The measurements at other times are not reliable because of poor reflectivity.

We expect the flux of momentum in the direction of the surface wind to be negative (downward), and the results shown here support that expectation. The wind-aligned component is generally negative. The crosswind component is often significant, although smaller than the wind-aligned component. This nonnegligible magnitude may be because the wind direction used to resolve the two components is that at 160–330 m, not at the surface.

The agreement between the fluxes computed from the clear-air and acoustic velocities is sometimes good, especially in the crosswind component. At other times and in the wind-aligned component, the acoustic measurement gives a much smaller magnitude than the clear-air measurement. Several reasons could account for this discrepancy. These are two largely independent measures of the flux, each with its own set of potential errors. For example, ground clutter and targets such as birds and aircraft affect the clear-air velocities but not the acoustic velocities. Peters (1991) shows that the momentum flux measured by the RASS includes a term proportional to the horizontal turbulent heat flux:

$$-\frac{\overline{C_a' u'}}{\cos\theta}, \tag{8}$$

where C_a is the acoustic velocity. We have neglected this term, which should be a few percent or less. For the subresolution calculation, Peters (1991) again shows that the momentum flux has a term

$$-\frac{1}{2\cos\theta}\left(\frac{Ca}{T}\frac{\partial T}{\partial z}\frac{\partial \bar{u}}{\partial z}\right)\delta z, \tag{9}$$

where δz is the radial length of the radar resolution cell

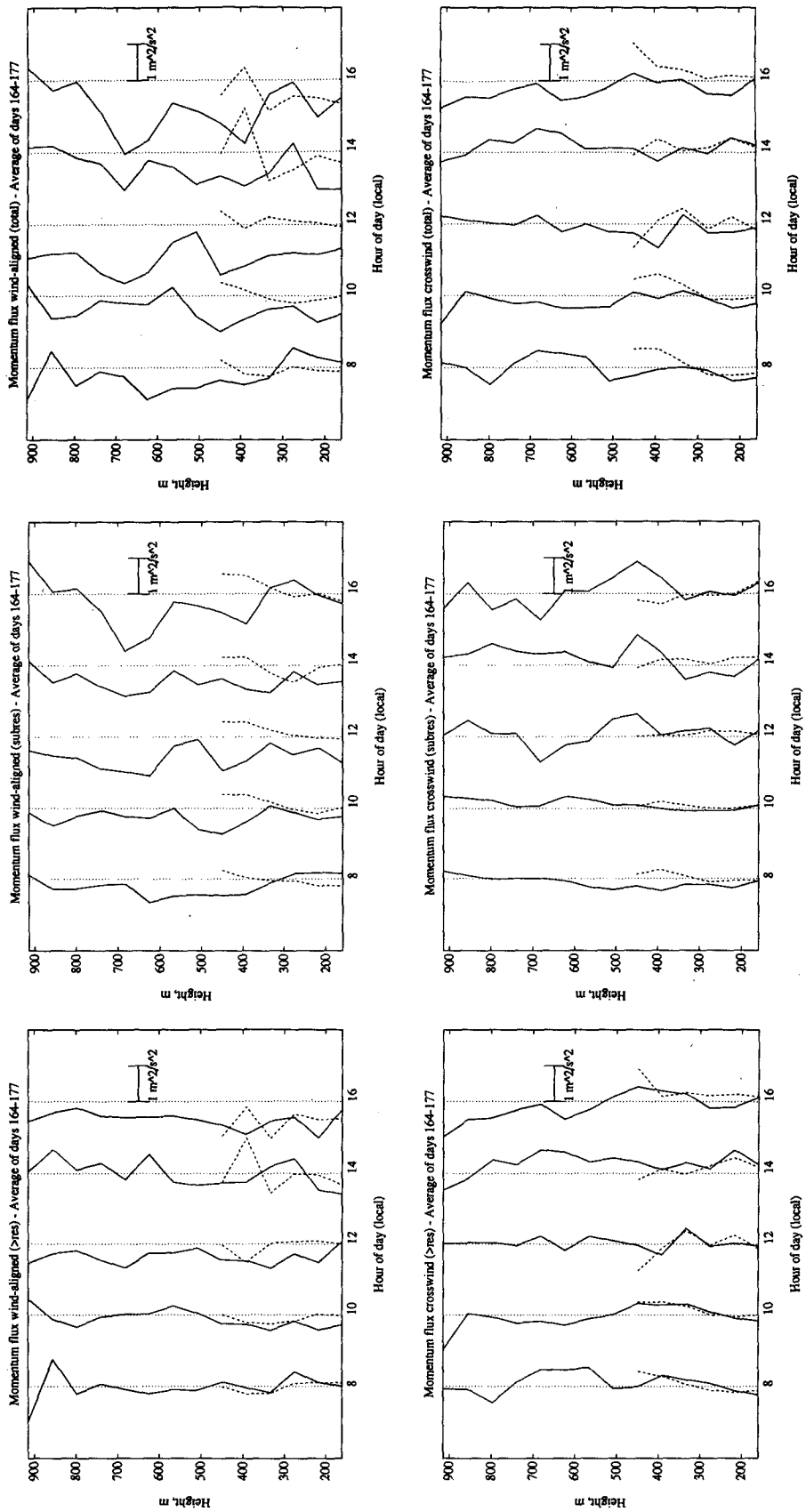

FIG. 6. Momentum flux. Solid lines are computed from the clear-air velocities; dashed lines are computed from the acoustic (RASS) velocities. Here (a) shows the flux on scales greater than the radar resolution volume; (b) shows the flux on scales less than the resolution volume; and (c) shows the total flux on all scales less than 2 h. Only averages over times from 0700 to 1700 are plotted due to unreliable data at other times.

(60 m in this case). Again, we have neglected this term here. The most likely source of error is that the beamwidth of the acoustic sources is comparable to the tilt angle of the radar antenna. This biases the RASS velocity measurements toward zero because the acoustic disturbance, and therefore the radar return, is strongest toward the zenith.

3. Error analysis

Figure 7 is a scatterplot of the heat flux during the 1100–1300 period. Each point is the flux measured during that period on one day. The solid line is the mean over the 14 days, and the dotted lines are the mean plus and minus one standard deviation. Figure 8 is the same plot for the momentum flux. The scatter may be due to differences between the days included in the composite, to the statistical behavior of the turbulence, or to measurement errors.

The expected variation due to the statistical behavior of the turbulence itself is given by Wyngaard (1992) as

$$\frac{t}{\tau} = 2\frac{F}{e^2}, \tag{10}$$

where t is the averaging time, τ is the integral scale of the turbulence, e is the fractional error, and

$$F = \frac{\overline{u^2}\,\overline{w^2} + \overline{u'w'}\,\overline{u'w'}}{\overline{u'w'}\,\overline{u'w'}}, \tag{11}$$

using a Gaussian approximation. The same relationship holds for heat flux if u' is replaced with T'. We can make a rough estimate of the error due to this variability. For the results presented here, t is 28 h. Taking the integral scale in space to be 500 m, using

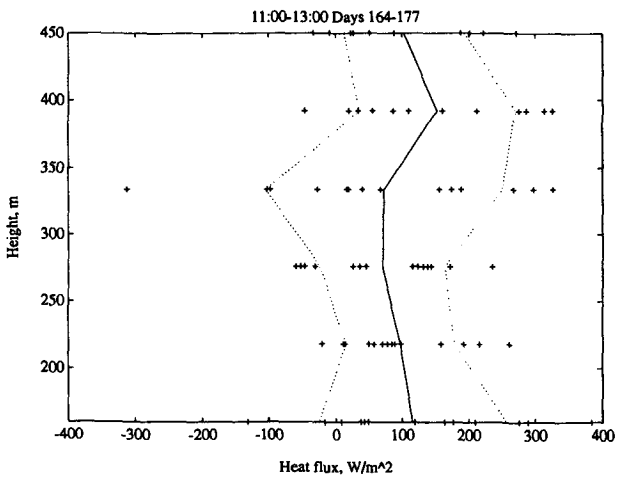

FIG. 7. Scatterplot of heat flux for the period 1100–1300. Individual points are the values for the 2-h period on each day. The solid line is the mean over the 14 days (with values outside ±400 W m^{-2} removed). The dotted lines are the mean plus and minus one standard deviation.

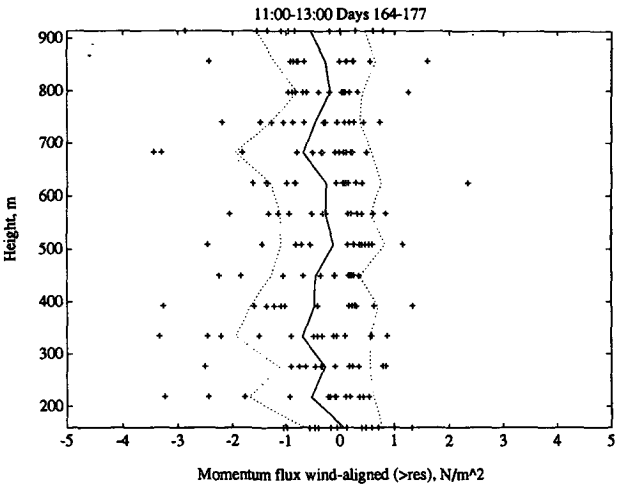

FIG. 8. Scatterplot of momentum flux for the period 1100–1300. Individual points are the values for the 2-h period on each day. The solid line is the mean over the 14 days (with values outside plus or minus 5 N m^{-2} removed). The dotted lines are the mean plus and minus one standard deviation.

the measured mean wind to convert this to the time integral scale τ, and computing F from the mean fluxes in the 1100–1300 period gives a fractional error e of 1 for the heat flux, and 0.4 for the momentum flux on scales greater than the radar resolution. In other words, the expected standard deviation due solely to atmospheric variability is about equal to the mean for the heat flux and slightly less than half the mean for the momentum flux. This is only an estimate of the error due to atmospheric variability because we do not have a direct measurement of the integral scale (which would be subject to similar uncertainty) and because the estimate depends on the uncertain measurement itself (F depends on $\overline{u'w'}$). It is nonetheless suggestive that the error estimated by this method is comparable to the standard deviation shown on the scatter plots.

A study of the accuracy of temperature measurements with RASS (May et al. 1989) compared RASS temperature profiles to those obtained with radiosondes. The results show that the accuracy of the RASS was comparable to that of the sondes, with rms differences of about 1.0°C. Much of that variation was thought to be due to the effects of vertical winds, which were not taken into account in that study. The authors indicate that an ultimate precision of 0.2°C or better can be achieved with vertical wind correction, as used in the experiment reported here.

4. Conclusions

Measurements of heat and momentum flux in the planetary boundary layer can be made with the 915-MHz wind profiler equipped with RASS. The quality of the measurements is limited during some times of

day because of poor radar reflectivity. A more sensitive radar would improve these measurements. Momentum fluxes derived from the clear-air radar signal and from acoustic velocities show encouraging agreement in some cases, notably in the crosswind component. The agreement would be improved significantly by using an acoustic source with a broader beamwidth. The calculation of second-order quantities, such as fluxes, is extremely sensitive to the quality of the data, and the most promising area for further investigation is in the improvement of algorithms for data quality control. Future work will include comparisons to flux measurements from aircraft.

Acknowledgments. Tzvi Gal-Chen and Gerhard Peters have contributed to this work through useful discussions. Richard Strauch and Ken Moran of the Wave Propagation Laboratory graciously permitted us to use the Platteville site and helped with logistics. Thanks to all who have had occasion to work at Platteville during this experiment for their toleration of the RASS acoustic "noise." This research was supported in part by the National Science Foundation under Agreement ATM-8720797.

REFERENCES

Angevine, W. M., W. L. Ecklund, D. A. Carter, K. S. Gage, and K. P. Moran, 1993: Improved radio acoustic sounding techniques. *J. Atmos. Ocean. Technol.*, **10,** in press.

Currier, P. E., W. L. Ecklund, J. M. Warnock, and B. B. Balsley, 1988: Temperature profiling using a UHF wind profiler and an acoustic source. *Proc. Lower Tropospheric Profiling: Needs and Technologies,* NCAR, NOAA WPL, and AMS, Boulder, CO, 121–122.

Ecklund, W. L., D. A. Carter, and B. B. Balsley, 1988: A UHF wind profiler for the boundary layer: Brief description and initial results. *J. Atmos. Oceanic Technol.*, **5,** 432–441.

Gal-Chen, T., M. Xu, and W. Eberhard, 1992: Estimations of ABL fluxes and other turbulence parameters from Doppler lidar data. *J. Geophys. Res.*, submitted.

Kaimal, J. C., J. C. Wyngaard, D. A. Haugen, O. R. Cote, Y. Izumi, S. J. Caughey, and C. J. Readings, 1976: Turbulence structure in the convective boundary layer. *J. Atmos. Sci.*, **33,** 2152–2169.

Kropfli, R. A., 1986: Single Doppler radar measurements of turbulence profiles in the convective boundary layer. *J. Atmos. Oceanic Technol.*, **3,** 305–314.

Matuura, N., Y. Masuda, H. Inuki, S. Kato, S. Fukao, T. Sato, and T. Tsuda, 1986: Radio acoustic measurement of temperature profile in the troposphere and stratosphere. *Nature,* **333,** 426–428.

May, P. T., R. G. Strauch, and K. P. Moran, 1988: The altitude coverage of temperature measurements using RASS with wind profiler radars. *Geophys. Res. Lett.*, **15,** 1381–1384.

——, K. P. Moran, and R. G. Strauch, 1989: The accuracy of RASS temperature measurements. *J. Appl. Meteor.*, **28,** 1329–1335.

——, R. G. Strauch, K. P. Moran, and W. L. Ecklund, 1990: Temperature sounding by RASS with wind profiler radars: A preliminary study. *IEEE Trans. Geosci. Remote Sens.*, **28,** 19–28.

NOAA, 1976: U.S. Standard Atmosphere. NOAA-S/T 76-1562, U.S. Government Printing Office, Washington, D.C.

North, E. M., and A. M. Peterson, 1973: RASS, a remote sensing system for measuring low-level temperature profiles. *Bull. Amer. Meteor. Soc.*, **54,** 912–919.

Peters, G., and H. J. Kertzel, 1992: Measurements of momentum flux in the boundary layer by RASS. *J. Atmos. Oceanic Technol.*, **9,** submitted.

——, H. Hinzpeter, and G. Baumann, 1985: Measurements of heat flux in the atmospheric boundary layer by sodar and RASS: A first attempt. *Radio Sci.*, **20,** 1555–1564.

Rabin, R. M., R. J. Doviak, and A. Sundara-Rajan, 1982: Doppler radar observations of momentum flux in a cloudless convective layer with rolls. *J. Atmos. Sci.*, **39,** 851–863.

Reid, I. M., 1987: Some aspects of Doppler radar measurements of the mean and fluctuating components of the wind field in the upper middle atmosphere. *J. Atmos. Terr. Phys.*, **49,** 467–484.

Stull, R. B., 1991: Static stability—An update. *Bull. Amer. Meteor. Soc.*, **72,** 1521–1529.

Vincent, R. A., and I. M. Reid, 1983: HF Doppler measurements of mesospheric gravity wave momentum fluxes. *J. Atmos. Sci.*, **40,** 1321–1333.

Wyngaard, V. C., 1992: Atmospheric turbulence. *Ann. Rev. Fluid Mech.*, **24,** 205–233.